

Online Adaptation of Monocular Depth Prediction with Visual SLAM

Shing Yan Loo^{1,2}, Moein Shakeri¹, Sai Hong Tang², Syamsiah Mashohor² and Hong Zhang¹

Abstract—The ability of accurate depth prediction by a CNN is a major challenge for its wide use in practical visual SLAM applications, such as enhanced camera tracking and dense mapping. This paper is set out to answer the following question: Can we tune a depth prediction CNN with the help of a visual SLAM algorithm even if the CNN is not trained for the current operating environment in order to benefit the SLAM performance? To this end, we propose a novel online adaptation framework consisting of two complementary processes: a SLAM algorithm that is used to generate keyframes to fine-tune the depth prediction and another algorithm that uses the online adapted depth to improve map quality. Once the potential noisy map points are removed, we perform global photometric bundle adjustment (BA) to improve the overall SLAM performance. Experimental results on both benchmark datasets and a real robot in our own experimental environments show that our proposed method improves the SLAM reconstruction accuracy. We demonstrate the use of regularization in the training loss as an effective means to prevent *catastrophic forgetting*. In addition, we compare our online adaptation framework against the state-of-the-art pre-trained depth prediction CNNs to show that our online adapted depth prediction CNN outperforms the depth prediction CNNs that have been trained on a large collection of datasets.

I. INTRODUCTION

Long-term adaptation in robotics is challenging yet invaluable for many practical applications, ranging from safe autonomous driving to human-robot interaction. In particular, we investigate the problem of visual SLAM with online adaptation by on-demand fine-tuning of a depth prediction convolutional neural network (CNN) and integrating online adapted depth prediction to improve structure and motion estimation.

Given a pre-trained depth prediction CNN—which may not necessarily perform well in a real-world setting—can we still integrate the CNN in a traditional SLAM pipeline such that the depth prediction CNN and the SLAM performance are simultaneously improved? To address this problem, we propose an on-demand adaptation framework. That is, we perform SLAM in an environment whose keyframes are used to determine the *quality* of predicted depth and, depending on the *quality*, we switch between fine-tuning of the depth prediction CNN and incorporating fine-tuned depth prediction into global bundle adjustment (BA) to improve SLAM accuracy. The main contributions of our work are as follows:

- We propose a novel online adaptation framework to fine-tune monocular depth prediction on-demand and

perform global BA to improve SLAM accuracy. Experimental results in real-world settings demonstrate an improvement in SLAM accuracy after incorporating online adapted depth in global photometric BA.

- To perform online adaptation of a depth prediction CNN, we introduce the use of CNN weight importance regularization, which has been shown to better retain the previously learned knowledge compared to using only *experience replay* [1]–[3].
- To improve the SLAM accuracy using the adapted depth prediction CNN, we propose using online adapted depth for culling the potential noisy map points before performing global photometric BA, resulting in an improvement of the reconstructed map.

II. RELATED WORK

To overcome the domain gap of single-image depth prediction, online learning has been used to fine-tune a depth prediction CNN on the images arriving sequentially [1], [2], [4], i.e., to fine-tune the CNN with the latest information available. One particular challenge for online fine-tuning is ensuring that learning does not overfit the most *recent* data, a problem known as *catastrophic forgetting* [5]. *Experience replay* has been proposed to mitigate *catastrophic forgetting* by inserting randomly sampled past training data into the current training batch [1]–[3]. An alternative solution is to regularize and preserve the CNN parameters that are important to the previously learned tasks [5], [6]. In a typical multi-task learning scenario, the importance of the CNN parameters can be measured by the magnitude of the gradients with respect to the loss function or output function through the training on a task [6]–[9], which intuitively determines how a perturbation in a CNN parameter affects the loss (see Appendix for more information). Instead of measuring the parameter importance after learning a task and regularizing the parameters in learning the next task, Maltoni and Lomonaco [9] propose single-incremental-task (SIT) learning, which seeks to estimate and consolidate the parameter importance from batch to batch using synaptic intelligence (SI), so that the previously learned knowledge is retained throughout the learning. Unlike SIT, which has to deal with learning new instances or classes, our goal is to preserve the previously learned depth from batch to batch by consolidating the parameter importance using a semi-supervised loss (instead of solving classification problems with ground truth labels [9]).

Depth prediction by a CNN has been widely used to benefit SLAM algorithms. To improve SLAM performance, a visual odometry (VO) pipeline can be enhanced by im-

¹The authors are with Department of Computing Science, University of Alberta, Canada.

²The authors are with Faculty of Engineering, Universiti Putra Malaysia, Malaysia.

proving feature matching [10] and photometric re-projection accuracies [11] through the use of depth prediction by CNNs. However, the predicted depth has to be accurate to achieve good performance, an assumption that is often violated in practical robotics applications. Therefore, instead of directly incorporating the predicted depth information into front-end tracking and mapping [10], [11], we design a VO pipeline that only incorporates online adapted depth information in optimizing the structure and motion estimation. To this end, we use two common procedures in SLAM optimization: map point culling and global BA. Removing noisy map points is an essential part of sparse SLAM for preventing erroneous state estimation from being included in optimization (cf. ORB-SLAM [12] and DSO [13]); on the other hand, global photometric BA [14], [15] has been shown to improve SLAM performance further. However, solving global BA can be expensive in terms of time and memory consumption [14]. Assuming that online fine-tuning can obtain reasonable depth prediction (without extreme accuracy), we use depth prediction as a hint to cull the potential noisy map points from being included in global photometric BA, resulting in accurate SLAM and light computational load.

III. METHOD

In this section, we outline our proposed online adaptation framework (see Figure 1). The framework consists of SLAM, online CNN depth adaptation, and global BA with adapted CNN depth.

A. SLAM

We use SVO 2.0¹ (its monocular variant with edgelets) to generate a set of keyframes from a monocular image stream captured by the camera on a mobile robot. Associated with each keyframe are an image, a camera pose, and a set of sparse map points. While the keyframes are being generated, we publish two serialized channels² over a local network containing the newly created keyframes (image, pose and map points) and keyframe graph (latest optimized camera poses and map points of all keyframes). The reason for publishing the keyframe graph is that local BA, in most cases, improves the camera pose estimation. Therefore, it is beneficial for improving the training loss in the online adaptation.

B. Online CNN depth adaptation

Our online adaptation is inspired by *early stopping*³ [16], whose goal is to avoid overfitting by stopping the fine-tuning when depth prediction is reasonably accurate, evaluated in terms of validation error (see Algorithm 1 for detailed steps).

To adapt a depth prediction CNN on sequential data without *forgetting*, we improve upon the *experience replay* method (i.e., incorporating *recent* data and randomly selecting *old* data into the training batches [1]–[3]) by adding

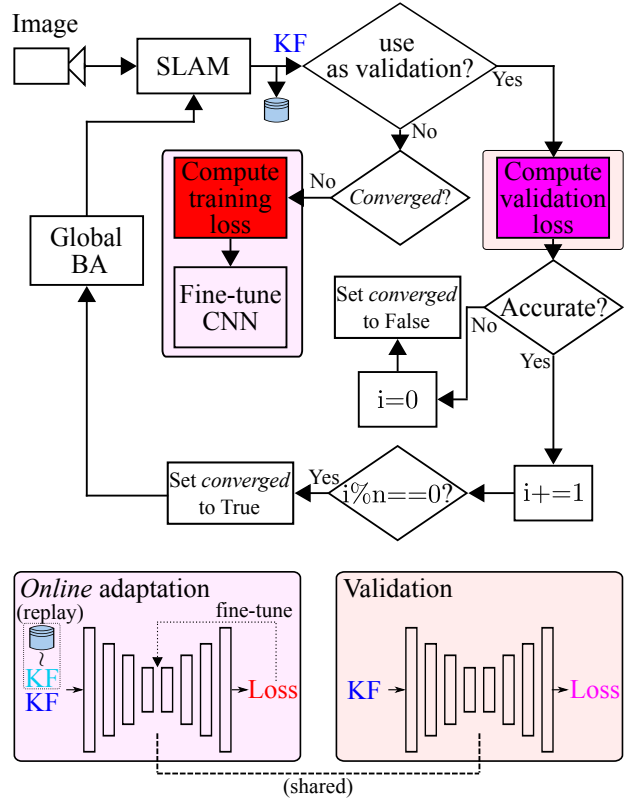


Fig. 1: Our proposed online adaptation framework. We use a SLAM algorithm to generate a sequence of keyframes. The keyframes are classified as training or validation to fine-tune a depth prediction CNN and monitor the adaptation progress. If the training is not converged, we use the most recent keyframe and one randomly sampled old keyframe to fine-tune the CNN. Meanwhile, we calculate the validation loss to determine if the predicted depth maps are accurate. We keep track of the number of continuous accurate depth predictions to perform global photometric BA if the CNN has been accurate for the past n keyframes. KF: keyframe.

regularization. Training regularization requires the consideration of the learning of two separate tasks \mathcal{T}_1 (learn from *old* data) and \mathcal{T}_2 (learn from *recent* data). The goal is to maximize the training accuracy on both \mathcal{T}_1 and \mathcal{T}_2 . To further reinforce the previously learned knowledge, we use EWC [6] regularization. Let θ^* be the CNN parameters fine-tuned on the last training batch and θ be the current CNN parameters. We introduce an additional regularization term to the training loss [6]:

$$\mathcal{L}_{\text{EWC}} = \mathcal{L}_{\text{train}} + \sum_i \frac{\beta}{2} \hat{F}_i (\theta_i - \theta_i^*)^2 \quad (1)$$

with

$$\begin{aligned} F &= F + F^j \\ \hat{F} &= \max\left(\frac{F}{j}, \max_F\right), \end{aligned} \quad (2)$$

where \hat{F}_i is the consolidated parameter importance matrix (also known as the diagonal of the Fisher information matrix) corresponding to the i -th parameter (see Appendix-A for more information) and \max_F determines the maximum value

¹https://github.com/HeYijia/svo_edgelet

²The keyframes are converted to ROS messages before they are published. See <http://wiki.ros.org/msg> for more information.

³https://www.tensorflow.org/api_docs/python/tf/keras/more_information

Algorithm 1 online adaptation framework represented in a finite-state machine

```

state = IDLE
t = 0
n_converged = 0
m = 5                                ▷ Validate every m steps
n = 3                                ▷ patience in the context of EarlyStopping
τ_val = 0.2                           ▷ Validation error threshold
while not done do
  if state == IDLE then
    run_global_ba = false
    if t > 0 and t % m == 0 then
      Compute validation error (L_val)
      if L_val < τ_val then
        n_converged += 1
      else
        n_converged = 0
      end if
      if n_converged > 0 and n_converged % n == 0 then
        run_global_ba = true
      end if
    else
      state = FINE_TUNE
    end if
  else if state == FINE_TUNE then
    Fine-tune the depth prediction CNN
    state = IDLE
  end if
  if run_global_ba then
    go through all keyframe and publish the keyframe
    depth maps to trigger BA in SVO
  end if
  t += 1
end while

```

of \hat{F} . Essentially, \hat{F} is an averaged parameter importance matrix to ensure the preservation of the previously learned knowledge.

To compute the training loss ($\mathcal{L}_{\text{train}}$), we use a *semi-supervised* training loss [17], [18], which consists of photometric re-projection ($\mathcal{L}_{\text{photo}}$), sparse depth ($\mathcal{L}_{\text{sparse_depth}}$) and smoothness loss ($\mathcal{L}_{\text{smooth}}$) terms:

1) *Photometric re-projection loss*:

$$\mathcal{L}_{\text{photo}} = \frac{1}{|V|} \sum_{p \in V} \min_s pe(I_i, I_{s \rightarrow i}), \text{ and} \quad (3)$$

$$pe(I_i, I_{s \rightarrow i}) = \frac{\alpha}{2} (1 - \text{SSIM}(I_i, I_{s \rightarrow i})) + (1 - \alpha) \|I_i - I_{s \rightarrow i}\|_1, \quad (4)$$

where $pe(\cdot, \cdot)$ is the minimum per-pixel photometric re-projection error [17] between the reconstructed images from the adjacent keyframes $I_s \in \{I_{i-1}, I_{i+1}\}$ and the i -th keyframe, and V a set of all valid re-projected pixel locations from the adjacent keyframes. To reconstruct the target image from an adjacent image $I_{s \rightarrow i}$, we use bilinear sampling at the valid (Ω_i) re-projected pixel locations p' using depth

Algorithm 2 Online fine-tuning with parameter importance regularization

```

1: Init  $\theta$  from a pre-trained depth prediction CNN
2:  $\hat{F} = 0$                                 ▷ parameter importance matrix
3: while not done do
4:    $\theta_{\text{cpy}} = \theta$                         ▷ Make a copy
5:   Get latest keyframe  $\mathcal{K}_i$  from SVO
6:   Train the CNN on  $\mathcal{K}_i$  and  $\mathcal{K}_{j \sim \{0, \dots, (i-1)\}}$  with  $\mathcal{L}_{\text{EWC}}$ 
     (see Eq. 1) according to  $\theta$  and  $\hat{F}$ 
7:   Consolidate the parameter importance matrix  $\hat{F}$  according to  $\theta_{\text{cpy}}$  and  $\theta$  (see Eq. 2)
8: end while

```

prediction $D_{i, \text{CNN}}$ and relative keyframe pose transformation $T_{i \rightarrow s}$ from SVO:

$$I_{s \rightarrow i}(p) = I_s(p') \quad \forall p \in \Omega_j, \quad (5)$$

$$p' \sim K T_{i \rightarrow s} D_{i, \text{CNN}}(p) K^{-1} p.$$

2) *Sparse depth loss*: We project the sparse map points generated by SVO in each keyframe to form sparse depth maps as *ground truth* labels [18], [19]

$$\mathcal{L}_{\text{sparse_depth}} = \frac{1}{|\Omega_{i, \text{sparse}}|} \sum_{p \in \Omega_{i, \text{sparse}}} \left| \frac{1}{D_{i, \text{CNN}}(p)} - \frac{1}{D_{i, \text{sparse}}(p)} \right|, \quad (6)$$

where $D_{i, \text{sparse}}$ is the sparse depth map of keyframe i , $\Omega_{i, \text{sparse}}$ a set of re-projected (sub)pixel locations containing depth values of their corresponding map points from SVO, and $|\Omega_{i, \text{sparse}}|$ the number of valid re-projections. By using inverse depth, near depth is penalized more heavily than far depth.

3) *Smoothness loss*:

$$\mathcal{L}_{\text{smooth}} = \frac{1}{N} \sum_p |\partial_x D_{i, \text{CNN}}(p)| e^{-|\partial_x I_i(p)|} + |\partial_y D_{i, \text{CNN}}(p)| e^{-|\partial_y I_i(p)|} \quad (7)$$

where ∂ is the gradient operator.

Combining the three loss terms, the final training loss is

$$\mathcal{L}_{\text{train}} = \mathcal{L}_{\text{photo}} + \lambda_1 \mathcal{L}_{\text{sparse_depth}} + \lambda_2 \mathcal{L}_{\text{smooth}}, \quad (8)$$

where λ_1 and λ_2 are the weighting parameters. Algorithm 2 details the steps involved in the online fine-tuning.

To validate the adaptation progress, we use the sparse depth loss term on all validation keyframes as the validation loss:

$$\mathcal{L}_{\text{val}} = \mathcal{L}_{\text{sparse_depth}}. \quad (9)$$

C. Global BA

To optimize the structure and motion, we employ the traditional photometric BA [15]. However, we found that the map points generated by SVO, albeit the sparsest amongst the state-of-the-art visual SLAM algorithms (cf. [12], [13]), still contain noisy and redundant map points. Therefore, with the learned depth information, we introduce a map point culling step before performing BA. To determine if a map point should be culled, we identify a host keyframe for the map

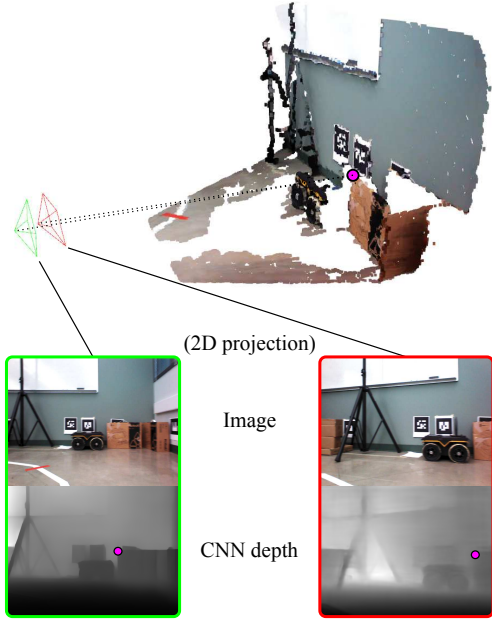


Fig. 2: Assuming the magenta map point is observed in two keyframes (the red and green camera frustums), a host keyframe is selected based on the validation loss (\mathcal{L}_{val}) of the predicted CNN depth, and in this case, the green keyframe has a lower \mathcal{L}_{val} and hence is being selected as the host keyframe of the magenta map point.

point (see Figure 2) and check if the depth of the map point is within the *correctness* range:

$$g(d_{mp}, d_{CNN}) = \begin{cases} 1, & \text{if } |d_{mp} - d_{CNN}| < \alpha d_{CNN} \text{ or} \\ & d_{CNN} > d_{max} \\ 0, & \text{otherwise} \end{cases} \quad (10)$$

where d_{CNN} and d_{mp} are the predicted CNN depth and the depth of the map point in the host keyframe, d_{max} a threshold that defines an *effective* depth range of the CNN depth values (similar to a depth sensor) to avoid far map points from being culled prematurely. $g(\cdot)$ evaluates if the map point is valid. Then, we use the standard photometric BA formulation [15] to optimize the structure and camera poses globally.

IV. EVALUATION

To evaluate the performance of our proposed method for online CNN adaptation experimentally, our mobile robot hardware setup consists of the following main components: a TurtleBot, an Nvidia Jetson AGX Xavier, an Orbbec Astra RGBD camera, and a laptop⁴, as shown in Figure 3. With the Jetson and laptop connected to the same wireless network, we run the SLAM process (tracking, mapping, and BA) on the Jetson and the fine-tuning process on the laptop.

To illustrate the effectiveness of the online adaptation, we use Monodepth2’s `mono+stereo_640x192` pre-trained CNN model, which has been trained on outdoor scenes fine-tuned in an indoor environment. For the network to learn, we use Adam optimizer with a learning rate of 10^{-3} , and set the

weighting of the loss function λ_1 , λ_2 and β at 0.1, 0.1 and 5×10^7 , respectively. For EWC consolidation of parameter importance matrix, \max_F is set to 0.001.

In SVO, the main change we made is the increased number of tracked features in the keyframes. We have modified the following parameter values: `max_fts` = 500, `grid_size` = 20, and `core_kfs` = 5. For performing map point culling, we define the *correctness* range by setting $\alpha = 0.5$ and $d_{max} = 1.5$. This particular design allows for more map points to be generated for fine-tuning the depth prediction CNN. The online adapted depth is then used for removing the potential noisy map points. After the noisy point removal, each map point has a maximum of five re-projection edges to the nearby keyframes, including the existing 3D-2D constraints (i.e., the list of observed keyframes for the map point), for performing global photometric BA in a separate thread. For each re-projection edge, we get a 3×3 image patch around the re-projected image coordinates to compute the photometric errors.

In the following, we present experimental results to validate the contributions of our proposed method. Section IV-A details the dataset that we collect in our laboratory and its purposes. Section IV-B compares and contrasts our proposed online adaptation method with regularization against the state-of-the-art methods. Section IV-C conducts an ablation study to compare different online adaptation schemes in overcoming *catastrophic forgetting*. Section IV-D presents quantitative and qualitative results of our proposed map point culling with online adapted depth and global photometric BA to improve map reconstruction accuracy. Section IV-E analyzes the accuracy of online adapted and pre-trained depth prediction to show the advantage of using online adaptation to improve SLAM performance.

A. Laboratory dataset

The reason for collecting our own dataset is that the image sequences in existing benchmarking datasets [20]–[22] are not long enough to evaluate and illustrate the effectiveness of our proposed online adaptation. Our dataset contains two sequences (dubbed Lab1 and Lab2) that we collected in our laboratory (see Figure 6 for the images of the captured environment). We record both sequences in the same environment, with the difference being the Lab2 sequence (16366 images) is longer than the Lab1 sequence (10611 images).

B. Online adaptation

To evaluate the effectiveness of our proposed online adaptation, we compare our method against the state-of-the-art methods: a SLAM-based approach by Luo et al. [4] (Section IV-B.1) and an end-to-end learning approach by Kuznetsov et al. [2] (Section IV-B.2). For the comparison, we follow the datasets and performance metric in [4]. The datasets are the ICL-NUIM [23] and TUM RGB-D [20] datasets and the performance metric is the percentage of overall depth pixels below 10% relative errors, i.e., $\frac{|D - D_{gt}|}{D_{gt}} < 0.1$.

⁴Specifications: Intel 7820HK CPU and Nvidia GTX 1070 GPU

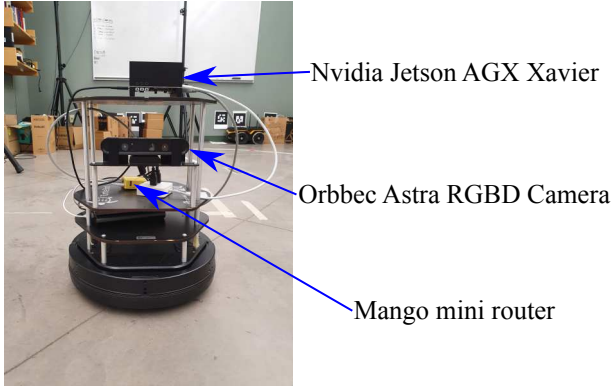


Fig. 3: A TurtleBot equipped with an Nvidia Jetson AGX Xavier and an Orbbec Astra RGBD camera. A Mango mini router is used to create a local wireless network to communicate between the Jetson and a laptop.

TABLE I: A comparison between the overall depth accuracy of our method and Luo et al.’s [4] SLAM-based online adaptation on the ICL-NUIM [23] and TUM RGB-D [20] datasets. (TUM/seq1: fr3_long_office_household, TUM/seq2: fr3_nostructure_texture_near_withloop, TUM/seq3: fr3_structure_texture_far)

Sequence	Percentage of correct depth (%)			
	Pre-trained [4]	[4]	Pre-trained	Ours
ICL/office0	19.117	22.206	8.766	12.541
ICL/office1	28.086	31.289	19.739	21.870
ICL/office2	21.695	21.695	4.591	42.244
ICL/living0	18.680	23.278	7.726	41.375
ICL/living1	21.071	22.774	8.518	49.075
ICL/living2	16.150	20.995	13.509	25.159
TUM/seq1	18.208	20.259	10.999	23.861
TUM/seq2	25.796	29.014	12.678	52.162
TUM/seq3	20.668	30.156	10.295	37.848
Average	21.052	24.630	10.758	34.015

1) *SLAM-based online adaptation:* Table I compares the overall depth accuracy between our method and a similar method by Luo et al. [4]. Our method improves the overall depth accuracy by around 23% (the last two columns), compared to 4% (2nd and 3rd column) by Luo et al. [4]. The performance gap could be due to the number of keyframes used in the fine-tuning; we use all the keyframes generated by SVO [24], whereas Luo et al. [4] use the keyframe pairs by LSD-SLAM [25] that have a dominant horizontal motion as simulated static stereo pairs. Besides, Luo et al. [4] perform online adaptation using most *recent* keyframes only, which performs the worst in the online adaptation scheme comparison (see Section IV-C). Note that Luo et al. [4] evaluate the keyframe depth accuracy based on the fine-tuned CNN models in different fine-tuning stages, which may result in different overall depth correctness should the final fine-tuned CNN model be used in the evaluation.

2) *Learning-based online adaptation:* Table II compares our method against a learning-based online adaptation method, CoMoDa⁵ [2]. Overall, our proposed SLAM-based method outperforms CoMoDa by around 5% (the last two

TABLE II: A comparison between the overall depth accuracy of our method and CoMoDa’s [2] end-to-end online adaptation on the ICL-NUIM [23] and TUM RGB-D [20] datasets. Both our method and CoMoDa [2] are fine-tuned on the same pre-trained CNN model, mono+stereo_640x192 [17]. (TUM/seq1: fr3_long_office_household, TUM/seq2: fr3_nostructure_texture_near_withloop, TUM/seq3: fr3_structure_texture_far)

Sequence	Percentage of correct depth (%)		
	Pre-trained*	Ours*	CoMoDa* [2]
ICL/office0	13.660	32.98	21.054
ICL/office1	22.453	38.383	41.623
ICL/office2	22.514	44.790	37.374
ICL/living0	17.659	48.158	35.164
ICL/living1	22.585	51.531	46.148
ICL/living2	21.606	35.757	35.571
TUM/seq1	16.931	27.915	33.120
TUM/seq2	17.722	41.782	33.708
TUM/seq3	23.026	50.339	39.769
Average	19.795	41.293	35.948

*Median scaling to ground truth depth

columns). One particular challenge in end-to-end online adaptation is the simultaneous fine-tuning of depth and pose prediction CNNs, and the pose prediction CNN is not trained in the tested indoor environments; on the contrary, we obtain camera poses from SVO [24]. And accurate camera pose estimation is essential when performing online adaptation (see Equation 5). Plus, CoMoDa does not use regularization in online adaptation, which is a reason that it performs worse than our method (see Section IV-C).

C. Learning against catastrophic forgetting in online adaptation

To evaluate the effectiveness of our proposed online adaptation, we perform an ablation study to measure the impact of different adaptation schemes on alleviating *catastrophic forgetting*. To this end, we examine the overall depth accuracy (using the same 10% relative error as the metric) on the ICL-NUIM [23] and TUM RGB-D [20] datasets.

Table III shows that performing online adaptation using only most *recent* keyframes has the worst overall depth accuracy (3rd column), compared to using the most *recent* keyframe with *experience replay* and regularization (the last two columns). Moreover, Figure 4 illustrates *catastrophic forgetting* on the lr_kt1 sequence, where the CNN is overfitted to the most *recent* keyframes in the sequence. In general, a combination of *experience replay* and regularization in online adaptation has the best overall depth accuracy (see the last column in Table III and Figure 4). Thus, it validates the effectiveness of our proposed online adaptation scheme. However, for a short sequence, regularization can inhibit changes in the CNN parameters and hurt the online adaptation accuracy (2nd last row in Table III). For the sake of completeness, we compare the online adaptation performances using the three popular regularization techniques⁷: EWC [6], MAS [7] and SI [8], and they perform similarly.

⁷See Appendix-B for more information. The regularization strength (λ in Eq. 17) for SI and MAS are set to 1.0 and 0.5, respectively.

⁵We generate results using CoMoDa’s [2] open-source code⁶

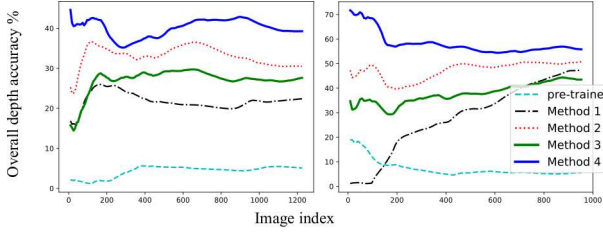


Fig. 4: A comparison of different online adaptation schemes tested on the ICL-NUIM [23] *of_kt3* (left) and *lr_kt1* (right) using the final online adapted CNN. Adaptation accuracy is measured by the averaged percentage of overall depth accuracy over all frames up to the frame. (Method 1: fine-tuning on most *recent* keyframes only; Method 2: fine-tuning on the most *recent* keyframe with *experience replay*; Method 3: fine-tuning on the most *recent* keyframe with regularization; Method 4: fine-tuning on the most *recent* keyframe with *experience replay* and regularization).

TABLE III: An ablation study on different online adaptation schemes using our proposed framework on the ICL-NUIM [23] and TUM RGB-D [20] datasets. (TUM/seq1: *fr3_long_office_household*, TUM/seq2: *fr3_nostructure_texture_near_withloop*, TUM/seq3: *fr3_structure_texture_far*)

Sequence	Percentage of correct depth (%)			
	Pre-trained	Ours(a)	Ours(b)	Ours(c)
ICL/office0	8.766	7.249	12.734	12.541
ICL/office1	19.739	4.034	22.613	21.870
ICL/office2	4.591	21.449	34.609	42.244
ICL/living0	7.726	13.179	22.883	41.375
ICL/living1	8.518	38.246	41.149	49.075
ICL/living2	13.509	9.110	13.117	25.159
TUM/seq1	10.999	16.012	19.782	23.861
TUM/seq2	12.678	14.457	37.539	52.162
TUM/seq3	10.295	49.515	51.545	37.848
Average	10.758	19.250	28.441	34.015

- (a) Online adaptation with two most *recent* keyframes
(b) Online adaptation with the most *recent* keyframe and *experience replay*
(c) Online adaptation with the most *recent* keyframe, *experience replay* and regularization

D. Effect of map point culling on reconstruction accuracy

After the depth prediction CNN has been fine-tuned to a reasonable accuracy, our following proposed method incorporates the online adapted depth into removing potential noisy map points and then performs photometric global BA to improve map reconstruction. To evaluate the correctness of the reconstructed map, we use the *Lab1* sequence with the percentage of correctly reconstructed map points in planar regions as the performance metric. Figure 5 the result in the two sets of walls (*Wall 1* and *Wall 2*). We can see that performing photometric BA alone does not guarantee improved map reconstruction accuracy, as minimizing photometric errors is still susceptible to local minima [26], [27]. By culling the potential outlier map points using the fine-tuned depth before performing photometric BA, the accuracy of the reconstructed map points on *Wall 2* is improved dramatically (also can be seen in Figure 6). The improved map reconstruction is based on the assumption that online adaptation can improve the depth prediction accuracy beyond the provided SVO sparse supervision, and we show (in

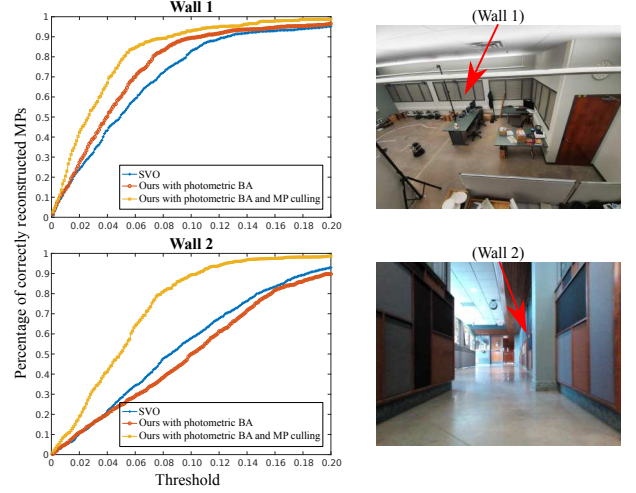


Fig. 5: Quantitative comparisons of the percentage of correctly reconstructed map points in two sets of selected map points on the *Lab1* sequence. The threshold determines the distance between a map point and a plane to be considered a *correct* map point. MP: map point.

Section IV-E) that this assumption is valid, especially with respect to performing online adaptation on a long sequence.

E. Online adaptation vs. relative depth prediction

A competing idea to our online adaption for resolving the domain gap in single-image depth prediction is to train a network with a large number of datasets across multiple domains to improve its generalization. Unlike absolute depth prediction, which is trained in a narrow domain, state-of-the-art relative depth prediction CNN models, such as MiDaS [28] and DiverseDepth [29], have been trained on an extensive collection of datasets. Therefore, to compare between online adapted depth and pre-trained depth prediction, we use the scale-invariant inverse depth error as the performance metric [30] given by:

$$e_{si} = \sqrt{\frac{1}{N} \sum_i d_i^2 - \frac{1}{N^2} (\sum_i d_i)^2} \quad (11)$$

where $d_i = \log z_i - \log z_i^*$, and the superscript $*$ indicates the ground truth depth. We perform the evaluation on the *Lab1* and *Lab2* sequences.

Table IV shows a quantitative comparison of the scale-invariant depth errors of sparse SVO map points, MiDaS, DiverseDepth and our fine-tuned Monodepth2 CNN model. On both sequences (2nd and 3rd column), our method has the lowest scale-invariant inverse depth error in comparison with the relative depth prediction CNNs⁸ (MiDaS and DiverseDepth) (see Figure 7 for a qualitative comparison). Due to the similarity between *Lab1* and *Lab2*, the depth prediction errors of MiDaS, DiverseDepth and pre-trained Monodepth2 are similar in both sequences. On the other hand, our method can further boost the depth prediction

⁸For relative depth prediction to achieve maximum accuracy, accurate scale- and shift-correction for each predicted depth map is required [29], [31]

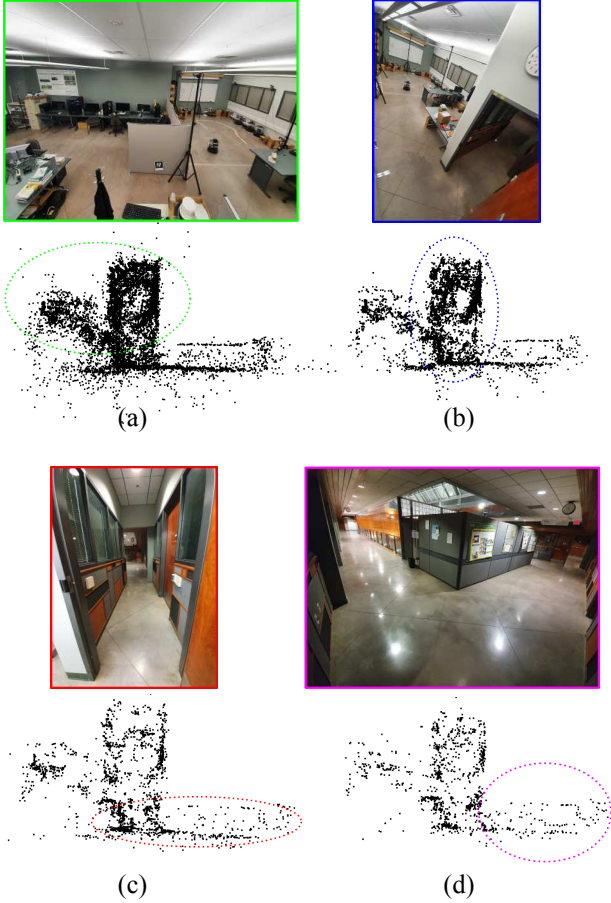


Fig. 6: Qualitative comparison between different *correctness* thresholds used in map point (MP) culling: (a) no culling, (b) MP culling with $\alpha = 0.5$, (c) MP culling with $\alpha = 0.25$ and (d) MP culling with $\alpha = 0.15$.

TABLE IV: A comparison of scale-invariant depth errors of SVO [24] map points, MiDaS [28], DiverseDepth [29] and our online adapted Monodepth2 [17] CNN model.

Method	e_{si}	
	Lab1	Lab2
SVO [†]	0.488	0.417
MiDaS (v2.1)	0.271	0.256
MiDaS (v3.0)	0.315	0.322
DiverseDepth	0.450	0.435
Pre-trained	0.401	0.399
Ours	0.226	0.197

[†] only the re-projected (sub)pixels

accuracy and SVO map point accuracy (see the last and 1st row of Table IV) resulting from our proposed online adaptation and global photometric BA with map point culling on a longer sequence⁹.

V. CONCLUSIONS

In this paper, we have addressed a practical robotics problem concerning the use of single-image depth prediction to improve SLAM performance. Particularly, we have

⁹SVO generates 517 and 796 keyframes on the Lab1 and Lab2 sequence, respectively.

proposed a novel online adaptation framework in which the fine-tuning is enhanced with regularization for retaining the previously learned knowledge while the CNN is being trained continually. Also, we have demonstrated the use of fine-tuned depth prediction for map point culling before running global photometric BA, resulting in a more accurate map reconstruction than running global photometric BA with all the map points. Lastly, we have compared our online adaptation framework against state-of-the-art depth prediction CNNs that have been trained on a large number of datasets across domains, showing that our online adapted depth prediction CNN has a lower depth error, especially after performing online adaptation on a long sequence.

One main shortcoming is that SVO is a visual odometry system and is prone to drift over time. For long-term adaptation problems, it would be better to incorporate loop closure and establish feature correspondences among the closed-loop keyframes to enhance the map reconstruction accuracy while the CNN is being online adapted. In return, the long-term adapted depth prediction CNN can be used to improve the SLAM accuracy further.

APPENDIX

A. EWC regularization

Given two tasks \mathcal{T}_1 and \mathcal{T}_2 , the problem is to first fine-tune the parameters (θ) of a CNN on \mathcal{T}_1 and then fine-tune on \mathcal{T}_2 while keeping the accuracy of \mathcal{T}_1 as much as possible.

Let E be the loss function of the problem at hand and assuming E to be locally smooth, we may expand the function about θ_0 using Taylor series approximation:

$$E(\theta) = E(\theta_0) + J_{\theta}(\theta_0)(\theta - \theta_0) + \frac{1}{2!}(\theta - \theta_0)^T H_{\theta}(\theta_0)(\theta - \theta_0) + \text{h.o.t.}, \quad (12)$$

where $J_{\theta}(\theta_0)$ and $H_{\theta}(\theta_0)$ are the Jacobian and Hessian of E evaluated at θ_0 , respectively. Assume that the CNN is fine-tuned on \mathcal{T}_1 , which implies that θ_0 would be at a local minimum (denoted by θ_0^*) and that $E'(\theta_0^*) = 0$, we can rewrite Equation 12 as

$$E^{\mathcal{T}_1}(\theta) \approx E(\theta_0^*) + \frac{1}{2!}(\theta - \theta_0^*)^T H_{\theta}(\theta_0^*)(\theta - \theta_0^*) \quad (13)$$

$$= E(\theta_0^*) + \frac{1}{2}J_{\theta}(\theta_0^*)^T J_{\theta}(\theta_0^*)(\theta - \theta_0^*)^2, \quad (14)$$

where $E^{\mathcal{T}_1}$ is the approximated error for \mathcal{T}_1 and $J_{\theta}^T J_{\theta}$ an approximation of H_{θ} [32].

Next, to fine-tune the CNN on \mathcal{T}_2 , we can use the following loss function:

$$E(\theta) = E^{\mathcal{T}_2}(\theta) + \beta E^{\mathcal{T}_1}(\theta), \quad (15)$$

where β controls the weighting between the two loss terms. Substituting Equation 14 into Equation 15, we get

$$\begin{aligned} E(\theta) &= E^{\mathcal{T}_2}(\theta) + \beta \left(E(\theta_0^*) + \frac{1}{2}J_{\theta}(\theta_0^*)^T J_{\theta}(\theta_0^*)(\theta - \theta_0^*)^2 \right) \\ &= E^{\mathcal{T}_2}(\theta) + \frac{\beta}{2} \left(J_{\theta}(\theta_0^*)^T J_{\theta}(\theta_0^*)(\theta - \theta_0^*)^2 \right), \end{aligned} \quad (16)$$

in which the first term of Equation 14 is being treated as a constant and can be eliminated in the optimization.



Fig. 7: A qualitative comparison of the back-projected point clouds (shown in black) between (from left to right) ground truth depth with SVO map points (in blue), MiDaS v2.1, MiDaS v3.0, DiverseDepth, pre-trained Monodepth2, and our online adapted Monodepth2. From top to bottom: first and second viewpoint of the back-projected depth maps and the predicted depth maps by the aforementioned CNN models. The predicted depth maps are scaled to ground truth. Best viewed digitally.

B. SI and MAS regularizations

Similar to EWC regularization, SI and MAS can be expressed using the following loss function:

$$\mathcal{L} = \mathcal{L}_{\text{train}} + \lambda \sum_i \Omega_i (\theta_i - \theta_i^*)^2, \quad (17)$$

with the main difference being the estimation of the weight importance matrix, Ω_i . For MAS, the weight importance matrix is given by the gradient of the squared L_2 -norm of the CNN output function, G [7]:

$$\Omega_i = \frac{1}{N} \sum_{j=1}^N \frac{\partial \|G(x_j; \theta)\|_2^2}{\partial \theta_i}, \quad (18)$$

whereas for SI, the weight importance matrix is given by [8]:

$$\Omega_i = \sum_j \frac{\omega_{ij}}{(\Delta\theta_{ij})^2 + \xi}, \quad (19)$$

where ω_{ij} is the estimated per-parameter contribution to the total loss, and $\Delta\theta_{ij}$ the total *trajectory* of the parameter.

REFERENCES

- [1] Milo Knowles, Valentin Peretroukhin, W Nicholas Greene, and Nicholas Roy. Toward robust and efficient online adaptation for deep stereo depth estimation. In *International Conference on Robotics and Automation (ICRA)*. IEEE, 2021.
- [2] Yevhen Kuznetsov, Marc Proesmans, and Luc Van Gool. Comoda: Continuous monocular depth adaptation using past experiences. In *Proceedings of the IEEE/CVF Winter Conference on Applications of Computer Vision (WACV)*, pages 2907–2917, January 2021.
- [3] Zhenyu Zhang, Stéphane Lathuilière, Elisa Ricci, Nicu Sebe, Yan Yan, and Jian Yang. Online depth learning against forgetting in monocular videos. In *Proceedings of the IEEE/CVF Conference on Computer Vision and Pattern Recognition*, pages 4494–4503, 2020.
- [4] Hongcheng Luo, Yang Gao, Yuhao Wu, Chunyuan Liao, Xin Yang, and Kwang-Ting Cheng. Real-time dense monocular slam with online adapted depth prediction network. *IEEE Transactions on Multimedia*, 21(2):470–483, 2018.
- [5] German I Parisi, Ronald Kemker, Jose L Part, Christopher Kanan, and Stefan Wermter. Continual lifelong learning with neural networks: A review. *Neural Networks*, 113:54–71, 2019.
- [6] James Kirkpatrick, Razvan Pascanu, Neil Rabinowitz, Joel Veness, Guillaume Desjardins, Andrei A Rusu, Kieran Milan, John Quan, Tiago Ramalho, Agnieszka Grabska-Barwinska, et al. Overcoming catastrophic forgetting in neural networks. *Proceedings of the national academy of sciences*, 114(13):3521–3526, 2017.
- [7] Rahaf Aljundi, Francesca Babiloni, Mohamed Elhoseiny, Marcus Rohrbach, and Tinne Tuytelaars. Memory aware synapses: Learning what (not) to forget. In *Proceedings of the European Conference on Computer Vision (ECCV)*, pages 139–154, 2018.
- [8] Friedemann Zenke, Ben Poole, and Surya Ganguli. Continual learning through synaptic intelligence. In *International Conference on Machine Learning*, pages 3987–3995. PMLR, 2017.
- [9] Davide Maltoni and Vincenzo Lomonaco. Continuous learning in single-incremental-task scenarios. *Neural Networks*, 116:56–73, 2019.
- [10] Shing Yan Loo, Ali Jahani Amiri, Syamsiah Mashohor, Sai Hong Tang, and Hong Zhang. Cnn-svo: Improving the mapping in semi-direct visual odometry using single-image depth prediction. In *2019 International Conference on Robotics and Automation (ICRA)*, pages 5218–5223. IEEE, 2019.
- [11] Nan Yang, Rui Wang, Jorg Stuckler, and Daniel Cremers. Deep virtual stereo odometry: Leveraging deep depth prediction for monocular direct sparse odometry. In *Proceedings of the European Conference on Computer Vision (ECCV)*, pages 817–833, 2018.
- [12] Carlos Campos, Richard Elvira, Juan J Gómez Rodríguez, José MM Montiel, and Juan D Tardós. Orb-slam3: An accurate open-source library for visual, visual-inertial, and multimap slam. *IEEE Transactions on Robotics*, 2021.
- [13] Jakob Engel, Vladlen Koltun, and Daniel Cremers. Direct sparse odometry. *IEEE transactions on pattern analysis and machine intelligence*, 40(3):611–625, 2017.
- [14] Nikolaus Demmel, Maolin Gao, Emanuel Laude, Tao Wu, and Daniel Cremers. Distributed photometric bundle adjustment. In *2020 International Conference on 3D Vision (3DV)*, pages 140–149. IEEE, 2020.
- [15] Hatem Alismail, Brett Browning, and Simon Lucey. Photometric bundle adjustment for vision-based slam. In *Asian Conference on Computer Vision*, pages 324–341. Springer, 2016.
- [16] Lutz Prechelt. Early stopping-but when? In *Neural Networks: Tricks of the trade*, pages 55–69. Springer, 1998.
- [17] Clément Godard, Oisín Mac Aodha, Michael Firman, and Gabriel J Brostow. Digging into self-supervised monocular depth estimation. In *Proceedings of the IEEE/CVF International Conference on Computer Vision*, pages 3828–3838, 2019.
- [18] Ali Jahani Amiri, Shing Yan Loo, and Hong Zhang. Semi-supervised monocular depth estimation with left-right consistency using deep neural network. In *2019 IEEE International Conference on Robotics and Biomimetics (ROBIO)*, pages 602–607. IEEE, 2019.
- [19] Lokender Tiwari, Pan Ji, Quoc-Huy Tran, Bingbing Zhuang, Saket Anand, and Manmohan Chandraker. Pseudo rgb-d for self-improving monocular slam and depth prediction. In *European Conference on Computer Vision*, pages 437–455. Springer, 2020.
- [20] Jürgen Sturm, Nikolas Engelhard, Felix Endres, Wolfram Burgard, and Daniel Cremers. A benchmark for the evaluation of rgb-d slam systems. In *2012 IEEE/RSJ international conference on intelligent robots and systems*, pages 573–580. IEEE, 2012.
- [21] Nathan Silberman, Derek Hoiem, Pushmeet Kohli, and Rob Fergus. Indoor segmentation and support inference from rgbd images. In *European conference on computer vision*, pages 746–760. Springer, 2012.
- [22] Angela Dai, Angel X Chang, Manolis Savva, Maciej Halber, Thomas Funkhouser, and Matthias Nießner. Scannet: Richly-annotated 3d reconstructions of indoor scenes. In *Proceedings of the IEEE conference on computer vision and pattern recognition*, pages 5828–5839, 2017.
- [23] Ankur Handa, Thomas Whelan, John McDonald, and Andrew J Davison. A benchmark for rgb-d visual odometry, 3d reconstruction and slam. In *2014 IEEE international conference on Robotics and automation (ICRA)*, pages 1524–1531. IEEE, 2014.
- [24] Christian Forster, Zichao Zhang, Michael Gassner, Manuel Werlberger, and Davide Scaramuzza. Svo: Semidirect visual odometry for monocular and multicamera systems. *IEEE Transactions on Robotics*, 33(2):249–265, 2016.
- [25] Jakob Engel, Thomas Schöps, and Daniel Cremers. Lsd-slam: Large-scale direct monocular slam. In *European conference on computer vision*, pages 834–849. Springer, 2014.
- [26] Richard A Newcombe, Steven J Lovegrove, and Andrew J Davison. Dtm: Dense tracking and mapping in real-time. In *2011 international conference on computer vision*, pages 2320–2327. IEEE, 2011.
- [27] Chengzhou Tang and Ping Tan. Ba-net: Dense bundle adjustment networks. In *International Conference on Learning Representations*, 2018.
- [28] René Ranftl, Katrin Lasinger, David Hafner, Konrad Schindler, and Vladlen Koltun. Towards robust monocular depth estimation: Mixing datasets for zero-shot cross-dataset transfer. *arXiv preprint arXiv:1907.01341*, 2019.
- [29] Wei Yin, Xinlong Wang, Chunhua Shen, Yifan Liu, Zhi Tian, Songcen Xu, Changming Sun, and Dou Renyin. Diversedepth: Affine-invariant depth prediction using diverse data. *arXiv preprint arXiv:2002.00569*, 2020.
- [30] B. Ummenhofer, H. Zhou, J. Uhrig, N. Mayer, E. Ilg, A. Dosovitskiy, and T. Brox. Demon: Depth and motion network for learning monocular stereo. In *IEEE Conference on Computer Vision and Pattern Recognition (CVPR)*, 2017.
- [31] Shing Yan Loo, Syamsiah Mashohor, Sai Hong Tang, and Hong Zhang. Deeprelativedfusion: Dense monocular slam using single-image relative depth prediction. In *International Conference on Intelligent Robots and Systems (IROS)*. IEEE, 2021.
- [32] Shun-ichi Amari, Hyeyoung Park, and Kenji Fukumizu. Adaptive method of realizing natural gradient learning for multilayer perceptrons. *Neural computation*, 12(6):1399–1409, 2000.